American Mineralogist, Volume 74, pages 1307–1316, 1989

Crystal-structure analysis of a birefringent andradite

KATHLEEN J. KINGMA,* JAMES W. DOWNS
Department of Geology and Mineralogy, The Ohio State University, Columbus, Ohio 43210, U.S.A.

ABSTRACT

The crystal structure of a noncubic garnet of composition $And_{94}Gr_5Spess_1$ was refined from single-crystal X-ray diffraction intensities to $R_w = 2.4\%$ for 3145 observations unique under Laue group $\bar{1}$. Although the unit cell is metrically cubic, with $a = 12.048(1)$ Å, the space group for this optically anisotropic garnet is found to be $I\bar{1}$, a subgroup of $Ia\bar{3}d$. Partial long-range ordering of Fe^{3+} and Al over the eight symmetrically unique octahedral sites of the $I\bar{1}$ structure is found to be significant and is cited as a possible origin for the observed optical anisotropy.

INTRODUCTION

Since the garnet structure was first determined by Menzer (1926, 1928) to be cubic (space group $Ia\bar{3}d$), several silicate garnets, especially those of grossular-andradite composition (grandites), have been found to be optically and structurally noncubic. The origin for the optical anisotropy has been attributed to many factors, including (1) substitution of rare-earth cations for Ca (Blanc and Maisonneuve, 1973), (2) twinning (Ingerson and Barksdale, 1943), (3) residual strain from lattice mismatch at compositional, twin, or grain boundaries (Chase and Lefever, 1960; Lessing and Standish, 1973; Kitamura and Komatsu, 1978), (4) noncubic distribution of OH^- groups due to the hydrogarnet substitution (Aines and Rossman, 1984; Rossman and Aines, 1986; Allen and Buseck, 1988), and (5) ordering of Fe^{3+} and Al over the octahedral sites (Takéuchi and Haga, 1976; Takéuchi et al., 1982; Akizuki, 1984; Allen and Buseck, 1988).

Takéuchi et al. (1982) examined garnets of intermediate grossular-andradite composition that crystallized in space groups $I\bar{1}$ and *Fddd* with Fe^{3+} and Al ordering over the octahedral sites. Allen and Buseck (1988) found a garnet of near-end-member grossular composition having a slight almandine component ($Fe_3^{2+}Al_2Si_3O_{12}$) to crystallize in space group $I\bar{1}$ and have cation ordering over both the octahedral (Al and Fe^{3+}) and dodecahedral (Ca and Fe^{2+}) sites. Since it has been shown that both ordering and optical birefringence decrease with increasing temperature, cation ordering is seen as a direct cause for the optical anisotropy of grandite garnets (Takéuchi and Haga, 1976; Takéuchi et al., 1982; Allen and Buseck, 1988).

While cation ordering is generally accepted as one possible origin for the optical anisotropy of certain grandites, less is understood about the mechanisms that initially created the ordering. Gali (1983) and Akizuki (1984) have similarly proposed that ordering occurs during crystal growth because of the inequivalency of the [Y] sites on the growth faces, which causes preferential site selection by the Fe^{3+} and Al cations. However, Hatch and Griffen (1989) recently suggested that, in addition to a crystal-growth mechanism, ordering may occur as a temperature-induced phase transformation from a disordered $Ia\bar{3}d$ structure to an ordered, or partially ordered lower-symmetry structure of *Fddd* or $I\bar{1}$ symmetry.

It was the aim of this study to use single-crystal X-ray diffraction to examine the crystal structure of an optically noncubic andradite containing only a small amount of Al and to investigate to what extent the deviation from cubic symmetry may be ascribed to long-range order of Fe^{3+} and Al over the octahedral sites.

EXPERIMENTAL DETAILS

The andradite garnets, from a metamorphic skarn deposit in the Sonoma Range, Nevada, were obtained from Ernest G. Ehlers' personal collection at The Ohio State University. These Sonoma andradites are reddish-brown, measure up to 8 mm in diameter, exhibit aa dodecahedral habit, and are iridescent. The andradites display the lamellar texture described by other investigators (Hirai et al., 1982; Akizuki, 1984; Akizuki et al., 1984; Hirai and Nakazawa, 1982, 1986a, 1986b). Thin sections reveal that the garnets are optically anisotropic with alternating zones of variable birefringence.

Samples for single-crystal X-ray investigation were prepared by crushing the large garnets and mounting suitable fragments on glass fibers. Several of these fragments were then selected for possible X-ray study on the basis of their optical homogeneity and birefringence observed using a spindle stage (for description, see Bloss, 1981). The polyhedral fragment chosen for the X-ray measurements has approximate dimensions 70 × 80 × 90 μm with nine easily definable faces. The fragment is biaxial positive with $2V_Z = 66(1)°$, as determined by extinction data using the program EXCALIBR (Bloss and Riess, 1973). The X optical direction is coincident with the crystallographic zone $[1\bar{1}0]$, whereas $Y \wedge [001] = Z \wedge [110] =$

* Present address: Department of Earth and Planetary Sciences, The Johns Hopkins University, Baltimore, Maryland 21218, U.S.A.

0003–004X/89/1112–1307$02.00

12°. Although the indices of refraction were not determined, maximum birefringence is estimated to be less than 0.005. Table 1 summarizes the data for the crystal fragment chosen for X-ray measurements.

An ALR-SEMQ electron microprobe operating with an accelerating voltage of 15 kV and a beam current of 20 nA was used to determine the composition of the same polyhedral fragment used in the measurement of X-ray intensities. Results of the analyses taken at 150 points across the fragment indicate near-end-member andradite composition ($And_{94}Gr_5Spess_1$) with no apparent compositional zonation across the grain. Table 2 lists the average of the microprobe analyses. The chemical formula assumed during the crystal-structure refinement was $\{Ca_{0.99}Mn_{0.01}\}_3[Fe_{0.94}Al_{0.06}]_2(Si)_3O_{12}$.

Data collection and reduction

All X-ray diffraction data were collected on a Rigaku AFC-6R single-crystal diffractometer at 23 °C. Mo$K\alpha$ radiation (λ = 0.71069 Å) was generated with a Rigaku RU-200 rotating-anode generator (0.5-mm filament, 0.5-mm collimator) operating at 50 kV and 180 mA and monochromatized with pyrolytic graphite. Diffractometer setting angles for 18 reflections with $90 < 2\theta < 110°$ were used in a least-squares unit-cell and orientation-matrix refinement, yielding an idealized cubic cell with a = 12.048(1) Å, which agrees well with a value of a_{calc} = 12.05 Å, calculated from the regression formula of Novak and Gibbs (1971). Intensities were measured using ω–2θ step-scans to allow for manual intervention during data reduction. Three standard reflections were monitored after every 150 measurements to check for crystal movement and to monitor intensity fluctuations. A total of 5921 intensities, including standards, were measured. Preliminary data collection indicated that reflections that might violate the body-centering symmetry rule (*hkl*: $h + k + l = 2n$) were low-angle reflections having 2θ less than 20°. Data were therefore collected in two stages in order to limit the total collection time without sacrificing the completeness of the final data set. First, all nodes of the reciprocal lattice within the sphere of reflection with $0 < 2\theta < 20°$ were scanned. This was followed by the measurement of intensities within one octant of the sphere of reflection that satisfy the body-centering rule and have $20 < 2\theta < 100°$.

Data-reduction software of Blessing (1987) was used to evaluate the peak positions and widths, correct each step for Lorentz and polarization effects, and calculate integrated intensities and variances. The polyhedral fragment's shape and size were accurately characterized using a spindle stage and an image-splitting eyepiece prior to the absorption correction, which was done analytically using the program ABSORB (DeTitta, 1985). Because no significant deviation of intensity was noted during data collection (~10 d), these data were not corrected for time-dependent intensity fluctuations. Replicate and equivalent data were averaged under Laue groups $m\bar{3}m$ and $\bar{1}$. Finally, $|F_o|$ and $\sigma(|F_o|)$ were estimated from $|F_o|^2$ and $\sigma(|F_o|^2)$, using Bayesian statistics described by French and Oatley (1983) and French and Wilson (1978).

Of the original 5921 intensities, 5357 are unique under Laue group $\bar{1}$, and only 932 are unique under $m\bar{3}m$. None of the 209 measurements of reciprocal lattice points that violate the body-centering rule yielded significant intensities. These data and 27 observations found to be integrated incorrectly were eliminated from the averaged reflection list. The final data set therefore contains 5121 observations unique under Laue group $\bar{1}$, with 3145 having $|F_o| > 2\sigma(|F_o|)$. Data collection and reduction are summarized in Table 1.

RESULTS

Space-group determination

Although the refined unit cell is metrically cubic, the Sonoma andradite is optically noncubic. It was assumed that the optical anisotropy was due to an atomic arrangement that deviated from $Ia\bar{3}d$ symmetry. To maintain the atomic coordinates of the garnet structure, only subgroups of $Ia\bar{3}d$ may be considered in choosing refinement models that depart from $Ia\bar{3}d$ symmetry. Preliminary refinements in the $Ia\bar{3}d$ subgroups $I2_13$, $I2_12_12_1$, *Pbca*, and $P2_12_12_1$, which each lack a center of symmetry and/or body-centering, showed strong correlations between the positional parameters of oxygen atoms that are related in $Ia\bar{3}d$ by these symmetry operations, indicating that the proper space group must be a centrosymmetric body-centered subgroup of $Ia\bar{3}d$. This conclusion is supported by the results of the recent group theoretical analysis of Hatch and Griffen (1989), who predicted the subgroups of $Ia\bar{3}d$ that could describe an ordered grandite phase.

The function $\Sigma w(|F_o| - k|F_c|)^2$ was minimized by full-matrix least-squares refinements where k is a scale factor and $w = 1/\sigma^2(|F_o|)$. Refinements were completed in space group $Ia\bar{3}d$ and its subgroups $Ia\bar{3}$, *Ibca*, $I4_1/a$, *Fddd*, $R\bar{3}$ and $I\bar{1}$ using the program RFINE4 (Finger and Prince, 1975). Expansion coefficients for neutral-atom scattering-factor curves and the anomalous dispersion terms of Cromer and Liberman (1970) were taken from *International Tables for X-ray Crystallography* (1974).

The final refinement cycle for each space group varied scale factor, positional parameters of atoms on general positions, anisotropic temperature factors, and Fe^{3+} occupancies on the unique octahedral sites (with the exception of $Ia\bar{3}d$, which has only one unique octahedral position). During preliminary refinements, secondary extinction was not found to be significant, and therefore a correction was not attempted. Octahedral-site populations were constrained by the unit-cell contents obtained from the results of the microprobe analyses of the sample crystal. Since preliminary structure refinements including the occupancy of Ca did not show significant ordering over the unique dodecahedral sites, only octahedral-site occupancies were refined.

Using Hamilton's significance test (Hamilton, 1965),

TABLE 1. Crystal data

Color	reddish brown	
Unit-cell contents	$\{Ca_{0.99}Mn_{0.01}\}_3[Fe_{0.94}Al_{0.06}]_2(Si)_3O_{12}$	
Dimensions (mm)	~(0.07 × 0.08 × 0.09)	
Crystal volume (mm^3)*	4.77×10^{-4}	
Crystal mass (mg)*	1.83×10^{-3}	
Transmission factor range*	0.640–0.719	
Linear absorption coefficient, μ (cm^{-1})	54.54	
Formula weight (g)	505.31	
Density, ρ_{calc} ($g \cdot cm^{-3}$)	3.84	
Unit-cell dimensions		
a_{calc} (Å)†	12.05	
a_{obs} (Å)	12.048(1)	
V_{obs} (Å^3)	1748.8(4)	
Data collection		
Step-scan mode	ω–2θ	
Steps per scan	96	
Step size (°ω)	0.02	
Seconds per step	1.0	
Total no. of observations, including standards	5921	
Range of sin θ/λ (Å^{-1})	0.04–1.08	
Data averaging		
Laue group	$\bar{1}$	$m\bar{3}m$
R (%)‡	1.0	3.1
R_w (%)	1.3	2.0
No. of unique observations	5121	932
Final $I\bar{1}$ refinement		
All data:		
R (%)§	10.4	
R_w (%)	2.7	
No. of observations	5121	
Data with $\lvert F_o\rvert > 2\sigma(\lvert F_o\rvert)$:		
R (%)	6.8	
R_w (%)	2.4	
No. of observations	3145	
No. of parameters	260	
S**	2.12	

Note: Esd's in parentheses refer to last significant digit.

* Value from face definitions using the program ABSORB (DeTitta, 1985).

† $a_{calc} = 9.04(2) + 1.61(4)\langle r[X]\rangle + 1.89(8)\langle r[Y]\rangle$, the linear-regression formula of Novak and Gibbs (1971), using effective ionic radii of Shannon and Prewitt (1969).

‡ Internal agreement factors are of the form $R = (\Sigma|Y_i - Y|)/\Sigma Y$ and $R_w = [(\Sigma w(Y_i - Y)^2)/\Sigma wY^2]^{1/2}$, with $w = 1/\sigma^2(Y_i)$. Y is the average Lorentz, polarization, and absorption-corrected integrated intensity, and the summation is over all symmetry equivalents and replicate observations.

§ $R = (\Sigma||F_o| - |F_c||)/\Sigma|F_o|$, $R_w = [(\Sigma w(|F_o| - |F_c|)^2)/\Sigma w|F_o|^2]^{1/2}$, $w = 1/\sigma^2(|F_o|)$.

** $S = \Sigma[(||F_o| - |F_c||)/\sigma(|F_o|)]/(n - m)$.

TABLE 2. Average of chemical analyses

Oxide	Wt%	s*	Cations per 12 oxygens	Refinement formula
SiO_2	36.41	± 0.41	3.04	3.00
TiO_2	0.01	± 0.01	—	
Al_2O_3	1.22	± 0.23	0.12	0.12
Fe_2O_3	29.16†	± 0.35	1.83	1.88
MgO	0.02	± 0.02	—	
MnO	0.54	± 0.05	0.04	0.04
CaO	33.16	± 0.19	2.96	2.96
Na_2O	0.01	± 0.02	—	
K_2O	0.00	± 0.01	—	
Sum	100.54		7.99	8.00

* $s = [(1/(N - 1))\Sigma(x_i - x)^2]^{1/2}$ (Bevington, 1969), $N = 150$.

† Fe was determined as FeO and converted to Fe_2O_3 by multiplying by 1.1113, the ratio of the atomic weights of FeO and Fe_2O_3.

the addition of anisotropic temperature factors to the refinement was significant at the 0.05 confidence level for all space groups. At the same confidence level, the addition of the occupancy parameters to the anisotropic refinement was only significant for space groups $I\bar{1}$, *Fddd,* and $R\bar{3}$.

Since the R factors for the final refinement in $I\bar{1}$ were the lowest of all refinements, the significance test was then used to compare the results of the $I\bar{1}$ refinement with the results of the final refinements of each of the other space groups. At a 0.05 confidence level, the $I\bar{1}$ model (380 parameters, including Fe^{3+} occupancies and anisotropic temperature factors for all atoms) is significantly better than each of the other space-group models and thus was chosen as the space group for the Sonoma andradite.

Refinement of the $I\bar{1}$ structure

After determining the space group to be $I\bar{1}$, several methods were used to determine (1) whether the refined Fe^{3+} occupancies were stationary with respect to various portions of the data set and (2) which observations or set of observations had intensities that are not predicted by the chosen $I\bar{1}$ model.

Because the Sonoma andradite has so little Al, it was not immediately apparent if the refined site occupancies of the $I\bar{1}$ structure were physically meaningful. By doing many $I\bar{1}$ refinements, each using a different portion of the original averaged data set, it was hoped that the site occupancies would remain virtually unchanged, indicating a nonequivalence among octahedral sites.

First, many $I\bar{1}$ refinements were done using different sin θ/λ shells of the averaged data, where a "sin θ/λ shell" is defined as all of the allowed reflections that are within chosen upper and lower sin θ/λ limits. Two groups of refinements, which we label the "high-angle refinement series" and the "low-angle refinement series," were analyzed for variations in refined site-occupancy parameters. Both series start with a refinement using all data in the averaged reflection list. The high-angle refinement series then consists of 13 additional refinements, each using progressively less of the low-angle data starting with the removal of data with $0.04 < \sin\theta/\lambda < 0.05$ Å^{-1}. The low-angle refinement series consists of 11 additional refinements, each using less of the high-angle data starting with the removal of data with $1.05 < \sin\theta/\lambda < 1.08$ Å^{-1}.

In the high-angle refinement series, the Fe^{3+} occupancies remain constant until too many of the low-angle data have been removed, at about $(\sin\theta/\lambda)_{min} = 0.45$ Å^{-1} (Fig. 1 and Table 3)[1]. Similarly, results of the low-angle refinement series [Fig. 2 and Table 4 (see footnote 1)] also demonstrate that the Fe^{3+} occupancies are stable until too

[1] A copy of Tables 3, 4, and 9 may be ordered as Document AM-89-421 from the Business Office, Mineralogical Society of America, 1625 I Street, N.W., Suite 414, Washington, D.C. 20006, U.S.A. Please remit $5.00 in advance for the microfiche.

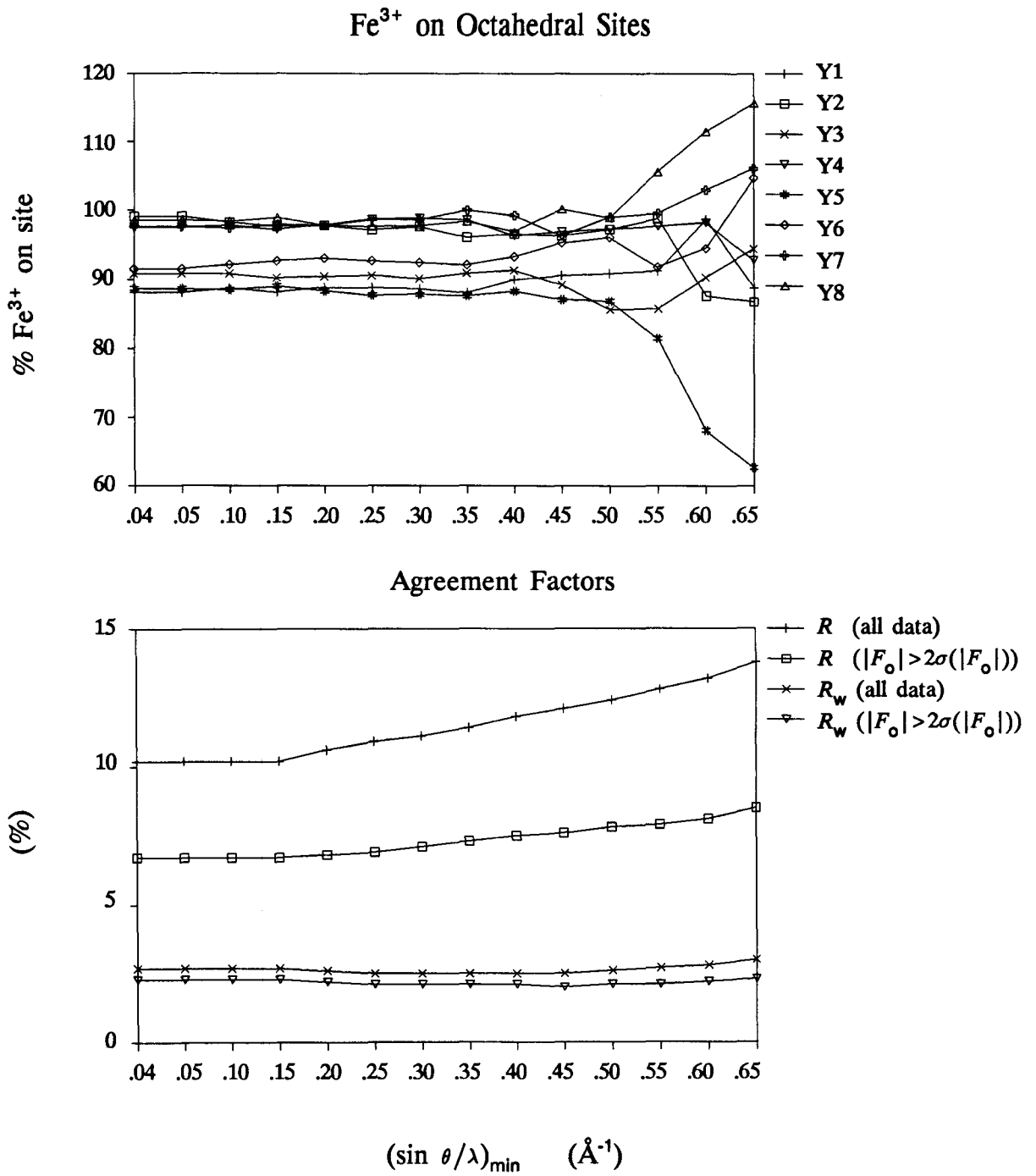

Fig. 1. Fe^{3+} occupancies and agreement factors from the $I\bar{1}$ high-angle refinement series. For each refinement, $(\sin \theta/\lambda)_{max} = 1.08$ Å^{-1}.

many of the high-angle data are removed at about $(\sin \theta/\lambda)_{max} = 0.75$ Å^{-1}.

In addition to these refinement series, separate $I\bar{1}$ refinements were done using (1) only those observations allowed by the $Ia\bar{3}d$ limiting conditions [$R_w = 2.1\%$ for the 3000 observations having $|F_o| > 2\sigma(|F_o|)$] and (2) only the low-intensity observations that are allowed by the $Ia\bar{3}d$ limiting conditions [$R_w = 5.9\%$ for the 2398 observations having $|F_o| > 2\sigma(|F_o|)$ and $|F_o|/k < 100$, where $k = 0.1292(1)$, the refined scale factor]. For both refinements, although only $Ia\bar{3}d$-allowed reflections were used, the same Fe^{3+} occupancies were refined as in the original $I\bar{1}$ refinement using all the data.

Because the Fe^{3+} occupancies do not vary as a function

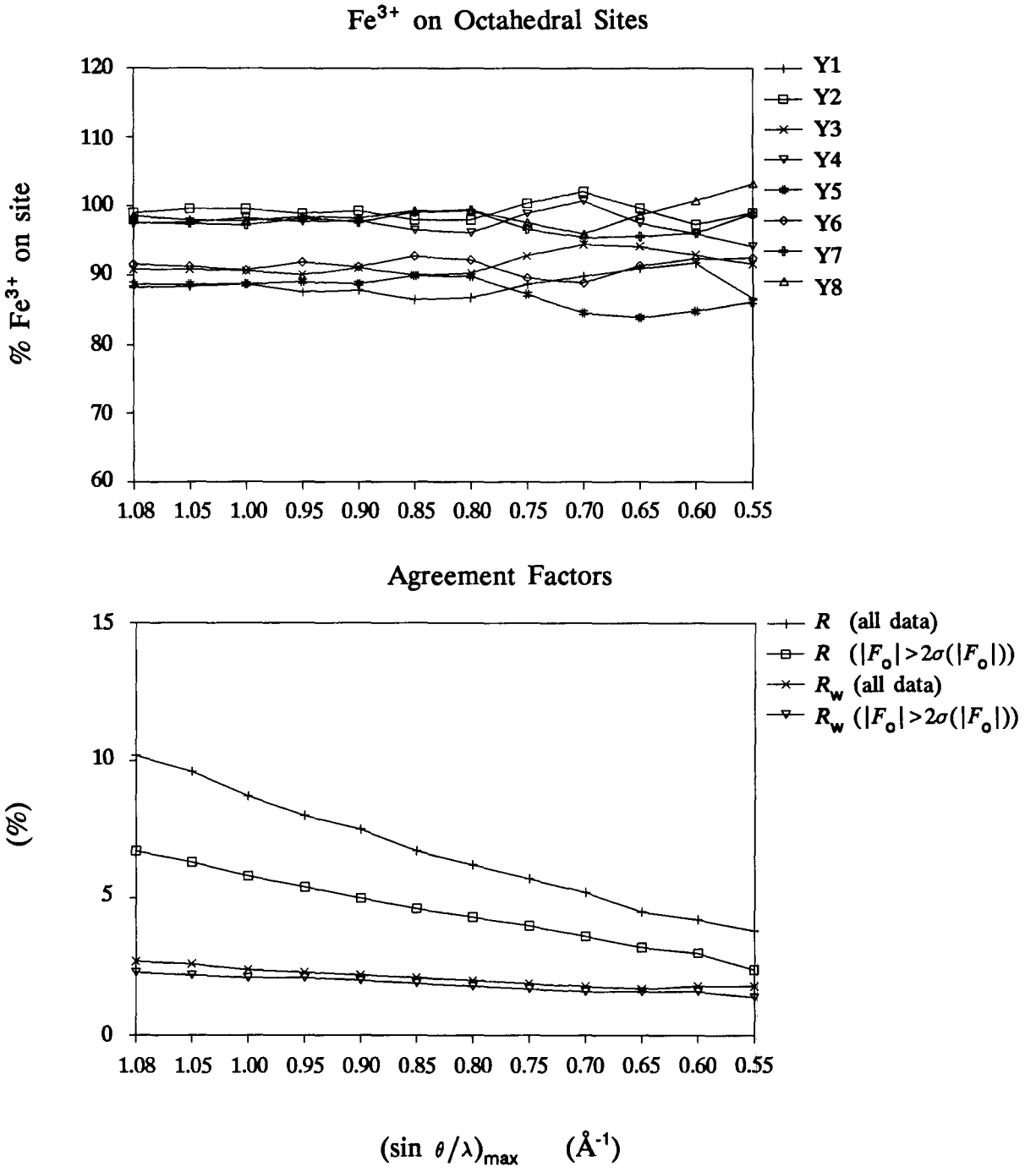

Fig. 2. Fe^{3+} occupancies and agreement factors from the $I\bar{1}$ low-angle refinement series. For each refinement, $(\sin\theta/\lambda)_{min} = 0.04$ Å^{-1}.

of the data used for refinement, as indicated by the results of the high-angle and low-angle refinement series and the $I\bar{1}$ refinements using only $Ia\bar{3}d$-allowed observations, we assume that the garnet has actual partial long-range ordering over the octahedral sites.

It is very interesting to note that the Sonoma andradite follows the ordering scheme predicted by Hatch and Griffen (1989). They concluded that if the ordering seen in many grandite garnets is the result of a homogeneous temperature-induced order-disorder phase transformation, the cation ordering of the $Ia\bar{3}d$ subgroup $I\bar{1}$ could be governed by both the T_{1g} and T_{2g} irreducible representations of $Ia\bar{3}d$. However, the observed ordering of both the Sonoma andradite and the $I\bar{1}$ Munam grandite from

TABLE 5. Fe^{3+} ordering in the $I\bar{1}$ garnet structure

Site	Munam grandite*		Sonoma andradite			
	Site label‡	Observed Fe^{3+} (%)	Site label	Oberved Fe^{3+} (%) (isotropic refinement)	Observed Fe^{3+} (%) (anisotropic refinement)	Ordering function for T_{2g}†
(0 0 0)	M(11)	41	Y1	87(1)	88(1)	$\eta_1 + \eta_2 + \eta_3$
(½ 0 ½)	M(12)	45	Y3	89(1)	91(1)	$\eta_1 - \eta_2 - \eta_3$
(0 ½ ½)	M(22)	29	Y2	97(1)	99(1)	$-\eta_1 - \eta_2 + \eta_3$
(½ ½ 0)	M(21)	15	Y4	96(1)	98(1)	$-\eta_1 + \eta_2 - \eta_3$
(¾ ¼ ¼)	M(14)	49	Y6	93(1)	92(1)	$\eta_1 - \eta_2 - \eta_3$
(¾ ¾ ¾)	M(13)	45	Y5	90(1)	89(1)	$\eta_1 + \eta_2 + \eta_3$
(¼ ¼ ¾)	M(23)	27	Y8	100(1)	99(1)	$-\eta_1 - \eta_2 + \eta_3$
(¼ ¾ ¼)	M(24)	16	Y7	100(1)	98(1)	$-\eta_1 + \eta_2 - \eta_3$

* Results from Takéuchi et al. (1982).
† From Hatch and Griffen (1989).
‡ Although the site labels are those of Takéuchi et al. (1982), the associated site coordinates are based on the unit-cell orientation of this study and of Hatch and Griffen (1989), such that *a*(Munam) = *b*(Sonoma), *b*(Munam) = *c*(Sonoma), and *c*(Munam) = *a*(Sonoma).

TABLE 6. Atomic positional parameters and isotropic temperature factors

Atom	*x*	*y*	*z*	B_{eq} or *B*
X1	0.1251(1)	0.0001(1)	0.2498(1)	0.49(4)
X2	0.2496(1)	0.1252(1)	0.0001(1)	0.52(4)
X3	−0.0001(1)	0.2498(1)	0.1252(1)	0.52(4)
X4	0.6250(1)	0.0001(1)	0.2501(1)	0.42(4)
X5	0.2499(1)	0.6250(1)	−0.0001(1)	0.41(4)
X6	0.0000(1)	0.2500(1)	0.6251(1)	0.40(4)
Y1	0.0	0.0	0.0	0.41(5)
Y2	0.0	0.5	0.5	0.34(4)
Y3	0.5	0.0	0.5	0.37(4)
Y4	0.5	0.5	0.0	0.25(4)
Y5	0.25	0.25	0.25	0.41(4)
Y6	0.25	0.75	0.75	0.35(4)
Y7	0.75	0.25	0.75	0.35(4)
Y8	0.75	0.75	0.25	0.38(4)
Si1	0.3751(2)	0.0000(2)	0.2501(2)	0.34(5)
Si2	0.2497(2)	0.3751(2)	−0.0001(2)	0.38(6)
Si3	−0.0001(2)	0.2498(2)	0.3751(2)	0.40(6)
Si4	0.8750(2)	0.0005(2)	0.2496(2)	0.48(6)
Si5	0.2496(2)	0.8753(2)	0.0000(2)	0.44(6)
Si6	−0.0001(2)	0.2498(2)	0.8755(2)	0.39(6)
O1	0.0391(3)	0.0490(3)	0.6556(3)	0.41(3)
O2	0.5391(4)	0.4523(4)	0.3451(4)	0.51(4)
O3	0.9604(3)	0.5493(3)	0.8446(3)	0.38(3)
O4	0.4612(4)	0.9519(4)	0.1550(4)	0.46(3)
O5	0.6551(3)	0.0383(3)	0.0495(3)	0.41(3)
O6	0.1553(4)	0.4612(4)	0.9516(4)	0.47(3)
O7	0.3450(4)	0.5393(4)	0.4516(4)	0.55(4)
O8	0.8442(3)	0.9607(3)	0.5491(3)	0.39(3)
O9	0.0490(4)	0.6549(3)	0.0396(4)	0.45(3)
O10	0.5486(4)	0.8448(3)	0.9600(4)	0.43(3)
O11	0.9507(4)	0.1555(4)	0.4607(4)	0.50(3)
O12	0.4519(4)	0.3449(4)	0.5396(4)	0.51(3)
O13	0.2891(4)	0.9057(4)	0.2989(4)	0.48(3)
O14	0.7894(4)	0.5950(4)	0.7021(4)	0.51(4)
O15	0.7101(4)	0.4058(4)	0.2010(4)	0.53(4)
O16	0.2109(3)	0.0948(3)	0.7983(3)	0.40(3)
O17	0.2989(4)	0.2887(4)	0.9055(4)	0.48(3)
O18	0.7990(3)	0.2107(3)	0.0943(3)	0.39(3)
O19	0.7013(4)	0.7900(4)	0.5946(4)	0.53(4)
O20	0.2012(4)	0.7107(4)	0.4059(4)	0.52(4)
O21	0.9052(4)	0.2995(4)	0.2885(4)	0.52(4)
O22	0.4049(4)	0.2015(4)	0.7114(4)	0.52(3)
O23	0.0943(4)	0.7991(4)	0.2107(4)	0.47(3)
O24	0.5947(4)	0.7018(4)	0.7894(4)	0.50(3)

Note: Isotropic temperature factors are reported for the oxygen atoms, whereas equivalent isotropic temperature factors [$B_{eq} = (4/3)a^2(\beta_{11} + \beta_{22} + \beta_{33})$] are reported for all cations.

Takéuchi et al. (1982) can only be described by the ordering function for T_{2g}, which predicts that the eight unique octahedral sites must divide into four sets of equivalently ordered sites (Table 5). Using the site labels of this study, these sets are Y1 and Y5, Y3 and Y6, Y2 and Y8, and Y4 and Y7.

To determine which observations, or set of observations, were contributing to the large difference between the weighted and unweighted *R* factors obtained from the first $I\bar{1}$ refinement, (1) *R* factors from the high-angle and low-angle $I\bar{1}$ refinement series were examined, and (2) *R* factors were calculated for certain subsets of observations from the structure-factor list calculated during the first $I\bar{1}$ refinement, which used all of the original averaged data.

Results of the high-angle refinement series [Fig. 1 and Table 3 (see footnote 1)] show that removal of the low-angle data leaves the weighted *R* factors unchanged while steadily worsening the unweighted *R* factors. Removal of the high-angle data in the low-angle refinement series also leaves the weighted *R* factors relatively unchanged, but steadily improves the unweighted *R* factors [Fig. 2 and Table 4 (see footnote 1)]. Since removal of the high-angle data, but not the low-angle data, reduces the difference between *R* and R_w by improving *R*, it was assumed that the large number of low-intensity observations, most of which are high-angle, in the complete data set are responsible for the discrepancy between the weighted and unweighted *R* factors.

To further test this theory, the structure-factor-amplitude list calculated during the $I\bar{1}$ refinement using all data was used to calculate *R* factors for specific groups of observations. Regardless of sin θ/λ, *all* of the relatively low intensity observations do not agree well with the chosen $I\bar{1}$ model [$R = 28.3\%$ and $R_w = 16.4\%$ for the 1823 observations with $|F_o|/k < 30$ and $|F_o| > 2\sigma(|F_o|)$], while *all* of the more intense observations are in good agreement [$R = 2.0\%$ and $R_w = 1.7\%$ for the 1322 observations with $|F_o|/k > 30$ and $|F_o| > 2\sigma(|F_o|)$]. Most of the low-intensity observations are also high-angle [1183 of the 1823 observations with $|F_o|/k < 30$ and $|F_o| > 2\sigma(|F_o|)$

TABLE 7. Apparent anisotropic-temperature-factor coefficients for cations

Atom	β_{11}	β_{22}	β_{33}	β_{12}	β_{13}	β_{23}
X1	0.0006(1)	0.0010(1)	0.0009(1)	0.0001(1)	−0.0002(1)	0.0001(1)
X2	0.0010(1)	0.0007(1)	0.0010(1)	0.0000(1)	0.0000(1)	0.0000(1)
X3	0.0008(1)	0.0012(1)	0.0007(1)	0.0001(1)	0.0002(1)	−0.0003(1)
X4	0.0005(1)	0.0010(1)	0.0007(1)	−0.0002(1)	0.0003(1)	0.0000(1)
X5	0.0008(1)	0.0005(1)	0.0008(1)	0.0002(1)	−0.0001(1)	0.0000(1)
X6	0.0009(1)	0.0008(1)	0.0004(1)	0.0000(1)	0.0000(1)	0.0002(1)
Y1	0.0007(1)	0.0008(1)	0.0006(1)	−0.0001(1)	0.0000(1)	−0.0001(1)
Y2	0.0004(1)	0.0005(1)	0.0009(1)	0.0003(1)	−0.0002(1)	−0.0001(1)
Y3	0.0008(1)	0.0006(1)	0.0004(1)	−0.0001(1)	−0.0001(1)	0.0001(1)
Y4	0.0004(1)	0.0006(1)	0.0003(1)	0.0001(1)	0.0002(1)	0.0001(1)
Y5	0.0007(1)	0.0007(1)	0.0008(1)	−0.0001(1)	−0.0002(1)	0.0000(1)
Y6	0.0006(1)	0.0009(1)	0.0003(1)	−0.0003(1)	0.0001(1)	0.0003(1)
Y7	0.0005(1)	0.0006(1)	0.0007(1)	0.0003(1)	0.0000(1)	−0.0001(1)
Y8	0.0008(1)	0.0007(1)	0.0005(1)	0.0001(1)	0.0001(1)	−0.0001(1)
Si1	0.0004(1)	0.0007(1)	0.0007(1)	0.0000(1)	0.0001(1)	−0.0002(1)
Si2	0.0005(1)	0.0007(1)	0.0008(1)	0.0002(1)	0.0000(1)	−0.0003(1)
Si3	0.0008(1)	0.0008(1)	0.0005(1)	0.0001(1)	−0.0002(1)	0.0002(1)
Si4	0.0009(1)	0.0008(1)	0.0008(1)	0.0000(1)	−0.0003(1)	0.0000(1)
Si5	0.0010(1)	0.0008(1)	0.0005(1)	−0.0003(1)	−0.0002(1)	0.0003(1)
Si6	0.0005(1)	0.0007(1)	0.0008(1)	0.0001(1)	0.0001(1)	−0.0002(1)

Note: The temperature factor in the structure-factor equation is of the form $T(\mathbf{h}) = \exp[-(h^2\beta_{11} + k^2\beta_{22} + l^2\beta_{33} + 2hk\beta_{12} + 2hl\beta_{13} + 2kl\beta_{23})]$.

have $\sin\theta/\lambda > 0.75$ Å^{-1} and $R = 30.1\%$ and $R_w = 29.8\%$), thus confirming the theory.

Although the Hamilton significance test indicated that the addition of anisotropic temperature factors for each atom to the $I\bar{1}$ refinement was significant over a refinement having only isotropic temperature factors, the anisotropic temperature factor coefficients for five of the oxygen atoms form a nonpositive definite matrix. Although the remaining oxygens had positive definite temperature factors, none was significantly positive within error. Since nonpositive definite anisotropic-temperature-factor coefficients represent a nonphysical probability-density function, all oxygens were constrained to vibrate isotropically.

The final refinement for which parameters are reported therefore varied scale factor, positional parameters for atoms on general positions, isotropic temperature factors for the 24 oxygens, anisotropic temperature factors for the 20 cations, and Fe^{3+} occupancies on the octahedral sites. Agreement factors (Table 1), Fe^{3+} site occupancies (Table 5), atomic positions and isotropic temperature factors (Table 6), apparent anisotropic-temperature-factor coefficients (Table 7), interatomic distances and angles (Table 8), and observed and calculated structure-factor amplitudes (Table 9; see footnote 1) are reported for the $I\bar{1}$ refinement using the complete averaged data set, which includes data with $0.04 < \sin\theta/\lambda < 1.08$ Å^{-1}.

DISCUSSION

It has been known for some time that certain garnets of the grossular-andradite solid-solution series may show noncubic optical and structural characteristics. This study represents the first crystal-structure analysis of an optically anisotropic garnet of near-end-member andradite composition, and, because the structures of garnets of grossular (Allen and Buseck, 1988) and intermediate grandite composition (Takéuchi et al., 1982) have previously been carefully studied, this research serves to broaden the knowledge of the noncubic behavior of garnets over the entire grandite solid-solution series.

Like the results of Allen and Buseck (1988) and Takéuchi et al. (1982), crystal-structure refinements suggest long-range cation ordering over the octahedral sites in the Sonoma andradite. This ordering of Fe^{3+} and Al defines eight symmetrically unique octahedral sites that are best described by an $I\bar{1}$ structure; the ordering may be responsible for the observed noncubic optical behavior of this garnet. However, without further characterization it may be premature to assume that long-range cation ordering is the only cause for the observed optical anisotropy of the Sonoma andradite. As demonstrated by Allen and Buseck (1988), the deviation from cubic symmetry of some grandites can be attributed to a complex origin, including not only long-range cation ordering, but also strain from twin-boundary lattice defects and noncubic distribution of OH^- groups. Although single-crystal X-ray diffraction suggests long-range cation ordering of the Sonoma andradite, further characterization using transmission electron microscopy and vibrational spectroscopy is in order.

ACKNOWLEDGMENTS

Microprobe analyses were performed at Virginia Polytechnic Institute and State University with the assistance of Todd Solberg. K.J.K. thanks Mickey Gunter and F. Donald Bloss of VPI & SU for assistance in the collection of extinction data. This work was submitted by K.J.K. to the Graduate School of The Ohio State University for the partial fulfillment of the requirements for the degree Master of Science and was supported by NSF Grant EAR-8618834 to J.W.D.

REFERENCES CITED

Aines, R.D., and Rossman, G.R. (1984) The hydrous component in garnets: Pyralspites. American Mineralogist, 69, 1116–1126.

TABLE 8. Interatomic distances (Å) and angles (°)

X1 dodecahedron							
X1-O1^{C}	2.359(5)	O1^{C}-O2^{D}	2.563(7)	65.9(2)	O7^{D}-O23^{A}	2.854(7)	69.7(2)
-O2^{D}	2.355(4)	O1^{C}-O8^{C}	2.880(4)	72.7(1)	O8^{C}-O13^{A}	2.920(7)	73.9(2)
-O7^{D}	2.598(5)	O1^{C}-O23^{A}	2.920(7)	73.9(2)	O8^{C}-O24^{B}	2.858(7)	69.7(1)
-O8^{C}	2.497(4)	O2^{D}-O7^{D}	2.866(8)	72.3(2)	O13^{A}-O14^{B}	2.562(7)	65.8(2)
-O13^{A}	2.355(5)	O2^{D}-O24^{B}	2.944(3)	74.5(1)	O13^{A}-O23^{A}	2.878(4)	72.7(1)
-O14^{B}	2.357(5)	O7^{D}-O14^{B}	2.944(3)	74.6(1)	O14^{B}-O24^{B}	2.875(7)	72.5(2)
-O23^{A}	2.495(4)						
-O24^{B}	2.503(5)						
Mean	2.440(5)					2839(6)	71.5(2)
X2 dodecahedron							
X2-O5^{C}	2.357(5)	O5^{C}-O7^{D}	2.574(7)	66.2(2)	O10^{C}-O17^{A}	2.931(7)	74.2(2)
-O7^{D}	2.360(5)	O5^{C}-O10^{C}	2.872(4)	72.4(1)	O12^{D}-O16^{A}	2.862(7)	69.8(2)
-O10^{C}	2.505(4)	O5^{C}-O16^{A}	2.922(6)	73.8(2)	O12^{D}-O19^{B}	2.943(3)	74.4(1)
-O12^{D}	2.501(5)	O7^{D}-O12^{D}	2.877(7)	72.5(2)	O14^{B}-O19^{B}	2.885(7)	72.6(2)
-O14^{B}	2.507(5)	O7^{D}-O14^{B}	2.944(3)	74.4(1)	O16^{A}-O17^{A}	2.873(4)	72.5(1)
-O16^{A}	2.503(4)	O10^{C}-O14^{B}	2.856(7)	69.5(2)	O17^{A}-O19^{B}	2.564(7)	65.9(2)
-O17^{A}	2.352(5)						
-O19^{B}	2.362(4)						
Mean	2.431(5)					2.842(6)	71.5(2)
X3 dodecahedron							
X3-O2^{D}	2.506(5)	O2^{D}-O12^{D}	2.876(7)	72.3(2)	O9^{C}-O12^{D}	2.571(7)	65.8(2)
-O3^{C}	2.494(4)	O2^{D}-O18^{A}	2.863(7)	69.9(2)	O9^{C}-O18^{A}	2.928(7)	74.0(2)
-O9^{C}	2.368(5)	O2^{D}-O24^{B}	2.944(3)	74.5(1)	O12^{D}-O19^{B}	2.943(3)	74.4(1)
-O12^{D}	2.363(5)	O3^{C}-O9^{C}	2.878(4)	72.5(1)	O18^{A}-O21^{A}	2.840(7)	72.7(1)
-O18^{A}	2.494(4)	O3^{C}-O19^{B}	2.843(7)	69.4(2)	O19^{B}-O24^{B}	2.879(7)	72.6(2)
-O19^{B}	2.501(5)	O3^{C}-O21^{A}	2.918(7)	74.0(2)	O21^{A}-O24^{B}	2.569(7)	66.1(2)
-O21^{A}	2.352(5)						
-O24^{B}	2.356(5)						
Mean	2.429(5)					2.838(6)	71.5(2)
X4 dodecahedron							
X4-O3^{B}	2.362(5)	O3^{B}-O4^{A}	2.568(5)	66.0(1)	O5^{A}-O21^{D}	2.856(5)	70.1(2)
-O4^{A}	2.356(3)	O3^{B}-O6^{B}	2.882(6)	72.6(2)	O6^{B}-O15^{D}	2.929(7)	74.0(2)
-O5^{A}	2.487(5)	O3^{B}-O21^{D}	2.918(7)	74.0(2)	O6^{B}-O22^{C}	2.868(4)	70.0(1)
-O6^{B}	2.499(5)	O4^{A}-O5^{A}	2.857(7)	72.2(2)	O15^{D}-O16^{C}	2.561(5)	65.7(1)
-O15^{D}	2.362(3)	O4^{A}-O22^{C}	2.935(7)	74.3(1)	O15^{D}-O21^{D}	2.878(7)	72.8(2)
-O16^{C}	2.357(5)	O5^{A}-O16^{C}	2.922(6)	74.1(2)	O16^{D}-O22^{C}	2.868(6)	72.3(2)
-O21^{D}	2.487(5)						
-O22^{C}	2.500(5)						
Mean	2.426(4)					2.837(6)	71.5(2)
X5 dodecahedron							
X5-O6^{A}	2.353(3)	O6^{A}-O8^{B}	2.562(5)	65.9(1)	O9^{A}-O18^{C}	2.928(7)	74.2(2)
-O8^{B}	2.359(5)	O6^{A}-O9^{A}	2.866(7)	72.4(2)	O11^{B}-O15^{C}	2.845(4)	69.5(1)
-O9^{A}	2.493(5)	O6^{A}-O15^{C}	2.929(7)	74.3(2)	O11^{B}-O20^{D}	2.921(7)	74.0(2)
-O11^{B}	2.492(5)	O8^{B}-O11^{B}	2.879(6)	72.8(2)	O13^{D}-O20^{D}	2.882(7)	72.8(2)
-O13^{D}	2.497(5)	O8^{B}-O13^{D}	2.920(7)	73.9(2)	O15^{C}-O18^{C}	2.886(6)	72.9(2)
-O15^{C}	2.496(5)	O9^{A}-O13^{D}	2.852(5)	69.7(2)	O18^{C}-O20^{D}	2.557(5)	65.7(1)
-O18^{C}	2.357(5)						
-O20^{D}	2.357(3)						
Mean	2.426(5)					2.836(6)	71.5(2)
X6 dodecahedron							
X6-O1^{A}	2.495(5)	O1^{A}-O11^{A}	2.881(7)	72.7(2)	O10^{B}-O11^{A}	2.568(5)	65.8(1)
-O4^{B}	2.503(5)	O1^{A}-O17^{D}	2.860(5)	69.9(2)	O10^{B}-O17^{D}	2.931(7)	74.1(2)
-O10^{B}	2.367(5)	O1^{A}-O23^{C}	2.920(7)	74.0(2)	O11^{A}-O20^{C}	2.921(7)	73.8(2)
-O11^{A}	2.361(3)	O4^{B}-O10^{B}	2.880(6)	72.5(2)	O17^{D}-O22^{D}	2.833(5)	72.4(2)
-O17^{D}	2.496(5)	O4^{B}-O20^{C}	2.864(4)	69.9(1)	O20^{C}-O23^{C}	2.886(7)	72.9(2)
-O20^{C}	2.498(5)	O4^{B}-O22^{D}	2.935(7)	74.3(2)	O22^{D}-O23^{C}	2.568(5)	66.0(1)
-O22^{D}	2.354(3)						
-O23^{C}	2.357(5)						
Mean	2.429(5)					2.837(6)	71.5(2)
Y1 octahedron*							
Y1-O2^{B}	2.009(5)	O2^{B}-O7^{B}	2.866(8)	90.1(2)	O2^{B}-O12^{D}	2.813(5)	88.7(2)
-O7^{B}	2.014(5)	O2^{B}-O7^{D}	2.822(5)	89.1(2)	O7^{B}-O12^{B}	2.876(7)	91.1(2)
-O12^{B}	2.014(4)	O2^{B}-O12^{B}	2.876(7)	91.3(2)	O7^{B}-O12^{D}	2.819(5)	88.9(2)
Mean	2.012(5)					2.845(6)	90.0(2)
Y2 octahedron*							
Y2-O4^{B}	2.011(5)	O4^{B}-O5^{B}	2.857(7)	90.4(2)	O4^{B}-O10^{D}	2.818(7)	88.8(2)
-O5^{B}	2.016(3)	O4^{B}-O5^{D}	2.838(5)	89.6(2)	O5^{B}-O10^{B}	2.872(4)	90.8(2)
-O10^{B}	2.018(4)	O4^{B}-O10^{B}	2.880(6)	91.2(2)	O5^{B}-O10^{D}	2.833(7)	89.2(2)
Mean	2.015(4)					2.850(6)	90.0(2)

TABLE 8—*Continued*

Y3 octahedron*							
Y3-O3^{B}	2.022(4)	O3^{B}-O6^{B}	2.882(6)	91.1(2)	O3^{B}-O9^{D}	2.832(7)	89.1(2)
-O6^{B}	2.015(5)	O3^{B}-O6^{D}	2.827(7)	88.9(2)	O6^{B}-O9^{B}	2.866(7)	90.6(2)
-O9^{B}	2.015(3)	O3^{B}-O9^{B}	2.878(4)	90.9(2)	O6^{B}-O9^{D}	2.834(5)	89.4(2)
Mean	2.017(4)					2.853(6)	90.0(2)
Y4 octahedron*							
Y4-O1^{B}	2.022(3)	O1^{B}-O8^{B}	2.880(4)	90.8(2)	O1^{B}-O11^{D}	2.838(5)	89.1(2)
-O8^{B}	2.024(4)	O1^{B}-O8^{D}	2.842(7)	89.2(2)	O8^{B}-O11^{B}	2.879(6)	90.7(2)
-O11^{B}	2.022(5)	O1^{B}-O11^{B}	2.881(7)	90.9(2)	O8^{B}-O11^{D}	2.843(7)	89.3(2)
Mean	2.023(4)					2.861(6)	90.0(2)
Y5 octahedron*							
Y5-O14^{B}	2.012(4)	O14^{B}-O19^{B}	2.885(7)	91.4(2)	O14^{B}-O24^{C}	2.822(5)	88.9(2)
-O19^{B}	2.021(5)	O14^{B}-O19^{C}	2.817(5)	88.6(2)	O19^{B}-O24^{B}	2.879(7)	91.0(2)
-O24^{B}	2.017(5)	O14^{B}-O24^{B}	2.875(7)	91.1(2)	O19^{B}-O24^{C}	2.831(5)	89.0(2)
Mean	2.017(5)					2.852(6)	90.0(2)
Y6 octahedron*							
Y6-O15^{B}	2.027(5)	O15^{B}-O18^{B}	2.886(6)	90.9(2)	O15^{B}-O21^{C}	2.840(5)	89.2(2)
-O18^{B}	2.024(4)	O15^{B}-O18^{C}	2.841(7)	89.1(2)	O18^{B}-O21^{B}	2.874(4)	90.7(2)
-O21^{B}	2.016(3)	O15^{B}-O21^{B}	2.878(7)	90.8(2)	O18^{B}-O21^{C}	2.840(7)	89.3(2)
Mean	2.022(4)					2.860(6)	90.0(2)
Y7 octahedron*							
Y7-O13^{B}	2.022(3)	O13^{B}-O20^{B}	2.882(7)	90.8(2)	O13^{B}-O23^{C}	2.843(7)	89.3(2)
-O20^{B}	2.025(5)	O13^{B}-O20^{C}	2.841(5)	89.2(2)	O20^{B}-O23^{B}	2.886(7)	90.9(2)
-O23^{B}	2.023(4)	O13^{B}-O23^{B}	2.878(4)	90.7(2)	O20^{B}-O23^{C}	2.839(7)	89.1(2)
Mean	2.023(4)					2.862(6)	90.0(2)
Y8 octahedron*							
Y8-O16^{B}	2.015(4)	O16^{B}-O17^{B}	2.873(4)	90.8(2)	O16^{B}-O22^{C}	2.826(7)	89.2(2)
-O17^{B}	2.019(3)	O16^{B}-O17^{C}	2.832(7)	89.2(2)	O17^{B}-O22^{B}	2.865(7)	90.6(2)
-O22^{B}	2.011(5)	O16^{B}-O22^{B}	2.868(6)	90.8(2)	O17^{B}-O22^{C}	2.833(5)	89.4(2)
Mean	2.015(4)					2.850(6)	90.0(2)
Si1 tetrahedron							
Si1-O3^{B}	1.645(3)	O3^{B}-O4^{A}	2.568(5)	102.4(2)	O4^{A}-O13^{A}	2.760(7)	113.6(2)
-O4^{A}	1.651(6)	O3^{B}-O13^{A}	2.750(4)	113.3(2)	O4^{A}-O14^{B}	2.754(7)	113.3(3)
-O13^{A}	1.647(5)	O3^{B}-O14^{B}	2.739(6)	112.6(2)	O13^{A}-O14^{B}	2.562(7)	102.1(3)
-O14^{B}	1.647(5)						
Mean	1.648(5)					2.689(6)	109.6(2)
Si2 tetrahedron							
Si2-O6^{A}	1.646(5)	O6^{A}-O8^{B}	2.562(5)	102.1(2)	O8^{B}-O17^{A}	2.755(4)	113.2(2)
-O8^{B}	1.647(3)	O6^{A}-O17^{A}	2.761(7)	113.7(2)	O8^{B}-O19^{B}	2.739(6)	112.8(2)
-O17^{A}	1.652(5)	O6^{A}-O19^{B}	2.744(7)	113.2(3)	O17^{A}-O19^{B}	2.564(7)	102.3(3)
-O19^{B}	1.641(6)						
Mean	1.647(5)					2.688(6)	109.6(2)
Si3 tetrahedron							
Si3-O10^{B}	1.644(3)	O10^{B}-O11^{A}	2.568(5)	102.6(2)	O11^{A}-O21^{A}	2.759(7)	113.3(2)
-O11^{A}	1.645(6)	O10^{B}-O21^{A}	2.749(4)	112.7(2)	O11^{A}-O24^{B}	2.754(8)	113.6(3)
-O21^{A}	1.658(5)	O10^{B}-O24^{B}	2.740(6)	112.8(2)	O21^{A}-O24^{B}	2.569(7)	102.1(3)
-O24^{B}	1.647(6)						
Mean	1.649(5)					2.690(6)	109.5(2)
Si4 tetrahedron							
Si4-O1^{C}	1.653(5)	O1^{C}-O2^{D}	2.563(7)	102.2(3)	O2^{D}-O15^{D}	2.753(8)	114.1(3)
-O2^{D}	1.642(6)	O1^{C}-O15^{D}	2.743(7)	112.9(2)	O2^{D}-O16^{C}	2.748(6)	113.2(2)
-O15^{D}	1.638(6)	O1^{C}-O16^{C}	2.747(4)	112.6(2)	O15^{D}-O16^{C}	2.561(5)	102.4(2)
-O16^{C}	1.650(3)						
Mean	1.646(5)					2.686(6)	109.6(2)
Si5 tetrahedron							
Si5-O5^{C}	1.661(5)	O5^{C}-O7^{D}	2.574(7)	102.4(3)	O7^{D}-O18^{C}	2.744(6)	113.1(2)
-O7^{D}	1.642(6)	O5^{C}-O18^{C}	2.759(4)	113.1(2)	O7^{D}-O20^{D}	2.751(8)	113.5(3)
-O18^{C}	1.645(3)	O5^{C}-O20^{D}	2.760(7)	113.2(2)	O18^{C}-O20^{D}	2.557(5)	102.0(2)
-O20^{D}	1.646(6)						
Mean	1.649(5)					2.691(6)	109.6(2)
Si6 tetrahedron							
Si6-O9^{C}	1.647(5)	O9^{C}-O12^{D}	2.571(7)	103.0(3)	O12^{D}-O22^{D}	2.754(7)	112.2(3)
-O12^{D}	1.639(5)	O9^{C}-O22^{D}	2.759(7)	113.1(2)	O12^{D}-O23^{C}	2.739(6)	112.9(2)
-O22^{D}	1.660(6)	O9^{C}-O23^{C}	2.752(4)	113.2(2)	O22^{D}-O23^{C}	2.567(5)	101.8(2)
-O23^{C}	1.649(3)						
Mean	1.649(5)					2.690(6)	109.4(2)

Note: Superscript letters next to oxygen atoms indicate $\bar{1}$ symmetry equivalent of refined position. Symmetry codes are as follows: $A = (X, Y, Z)$, $B = (-X, -Y, -Z)$, $C = (\frac{1}{2} + X, \frac{1}{2} + Y, \frac{1}{2} + Z)$, $D = (\frac{1}{2} - X, \frac{1}{2} - Y, \frac{1}{2} - Z)$.

* Each octahedral interatomic distance and each angle are related by twofold symmetry to another distance and angle that are not listed in the table.

Akizuki, M. (1984) Origin of optical variations in grossular-andradite garnet. American Mineralogist, 69, 328–338.

Akizuki, M., Nakai, H., and Suzuki, T. (1984) Origin of iridescence in grandite garnet. American Mineralogist, 69, 896–901.

Allen, F.M., and Buseck, P.R. (1988) XRD, FTIR, and TEM studies of optically anisotropic grossular garnets. American Mineralogist, 73, 568–584.

Bevington, P.R. (1969) Data reduction and error analysis for the physical sciences, 336 p. McGraw-Hill, New York.

Blanc, Y., and Maisonneuve, J. (1973) Sur la biréfringence des grenats calciques. Bulletin de la Société française de Minéralogie et de Cristallographie, 96, 320–321.

Blessing, R.H. (1987) Data reduction and error analysis for accurate single crystal diffraction intensities. Crystallography Reviews, 1, 3–58.

Bloss, F.D. (1981) The spindle stage: Principles and practice, 340 p. Cambridge University Press, Cambridge, England.

Bloss, F.D., and Riess, D. (1973) Computer determination of $2V$ and indicatrix orientation from extinction data. American Mineralogist, 58, 1052–1061.

Chase, A.B., and Lefever, R.A. (1960) Birefringence of synthetic garnets. American Mineralogist, 45, 1126–1129.

Cromer, D.T., and Liberman, D. (1970) Relativistic calculation of anomalous scattering factors for X rays. Journal of Chemical Physics, 53, 1891–1898.

DeTitta, G.T. (1985) ABSORB: An absorption correction program for crystals enclosed in capillaries with trapped mother liquor. Journal of Applied Crystallography, 18, 75–79.

Finger, L.W., and Prince, E. (1975) A system of Fortran IV computer programs for crystal structure computations. National Bureau of Standards Technical Note 854.

French, S., and Oatley, S. (1983) Bayesian statistics: An overview. In S. Ramaseshan, M.F. Richardson, and A.J.C. Wilson, Eds., Crystallographic statistics: Progress and problems, p. 19–51. Indian Academy of Sciences, Bangalore.

French, S., and Wilson, K. (1978) On the treatment of negative intensity observations. Acta Crystallographica, A34, 517–525.

Gali, S. (1983) Grandite garnet structures in connection with the growth mechanism. Zeitschrift für Kristallographie, 163, 43–52.

Hamilton, W.C. (1965) Significance tests on the crystallographic R factor. Acta Crystallographica, 18, 502–510.

Hatch, D.M., and Griffen, D.T. (1989) Phase transitions in grandite garnets. American Mineralogist, 74, 151–159.

Hirai, H., and Nakazawa, H. (1982) Origin of iridescence in garnet: An optical interference study. Physics and Chemistry of Minerals, 8, 25–28.

——— (1986a) Grandite garnet from Nevada: Confirmation of origin of iridescence by electron microscopy and interpretation of a moiré-like texture. American Mineralogist, 71, 123–126.

——— (1986b) Visualizing low symmetry of a grandite garnet on precession photographs. American Mineralogist, 71, 1210–1213.

Hirai, H., Sueno, S., and Nakazawa, H. (1982) A lamellar texture with chemical contrast in grandite garnet from Nevada. American Mineralogist, 67, 1242–1247.

Ingerson, E., and Barksdale, J.D. (1943) Iridescent garnet from the Adelaide mining district, Nevada. American Mineralogist, 28, 303–312.

International tables for X-ray crystallography. (1974) Volume IV. J.A. Ibers and W.C. Hamilton, Eds. Kynoch Press, Birmingham, England.

Kitamura, K., and Komatsu, H. (1978) Optical anisotropy associated with growth striation of yttrium garnet, $Y_3(Al,Fe)_5O_{12}$. Kristallographie und Technik, 13, 811–816.

Lessing, P., and Standish, R.P. (1973) Zoned garnet from Crested Butte, Colorado. American Mineralogist, 58, 840–842.

Menzer, G. (1926) Die Kristallstruktur von Granat. Zeitschrift für Kristallographie, 63, 157–158.

——— (1928) Die Kristallstruktur der Granate. Zeitschrift für Kristallographie, 69, 300–396.

Novak, G.A., and Gibbs, G.V. (1971) The crystal chemistry of the silicate garnets. American Mineralogist, 56, 791–825.

Rossman, G.R., and Aines, R.D. (1986) Spectroscopy of a birefringent grossular from Asbestos, Quebec, Canada. American Mineralogist, 71, 779–780.

Shannon, R.D., and Prewitt, C.T. (1969) Effective ionic radii in oxides and fluorides. Acta Crystallographica, B25, 925–945.

Takéuchi, Y., and Haga, N. (1976) Optical anomaly and structure of silicate garnets. Proceeding of the Japanese Academy, 52, 228–231.

Takéuchi, Y., Haga, N., Umizu, S., and Sato, G. (1982) The derivative structure of silicate garnets in grandite. Zeitschrift für Kristallographie, 158, 53–99.

Manuscript received April 24, 1989
Manuscript accepted July 26, 1989